

PRECURSORY AE PATTERNS LEADING TO ROCK FRACTURE

David A. Lockner and James D. Byerlee

U.S. Geological Survey
Menlo Park, CA, USA

ABSTRACT

Intact samples of granite and sandstone have been deformed to failure at 50 MPa confining pressure. In these experiments, the acoustic emission (AE) rate was used to control deviatoric stress on the sample. As a result, fault growth, which normally would occur unstably in a fraction of a second, was stabilized and extended to a matter of minutes and even hours. Inversion of AE arrival times at a set of transducers allowed for the three dimensional location of AE events during initial loading, fault nucleation and growth stages in each experiment. Fault nucleation occurred abruptly and after peak strength in all granite experiments, showing only subtle changes in clustering and other AE patterns prior to nucleation. Statistical analysis of AE locations and amplitudes showed systematic changes in b value and geometric parameters (in part related to fractal dimension) between peak stress and nucleation. The most consistently observed precursor was the development of a planar distribution of AE hypocenters near peak stress. The orientation of this AE pattern was associated with the macroscopic fault that eventually developed. These changes suggest that microcracking first began to organize in the granite samples near peak stress. Similar trends were observed in a sandstone experiment, although, in that case, clustering of AE events occurred well before peak stress. We interpret this early clustering in the sandstone sample to be the result of pre-existing strength heterogeneities. Finally, an increased probability was observed for the occurrence of sequential events separated by less than 5 mm.

INTRODUCTION

A new control technique has recently been presented [Lockner *et al.*, 1991a, b] which slows down the normally violent fault propagation in brittle rock so that faults can be grown quasi-statically. This growth stabilization technique, similar to one developed independently by Terada *et al.* [1984] employs a fast-acting servo control system to adjust axial stress so that an approximately constant acoustic emission (AE) rate is maintained. Combined with this technique, we have recorded arrival time and amplitude data of the naturally occurring AE events. Inversion of the arrival time data to determine

3-dimensional hypocentral locations provides information about the accumulation of microcrack damage during the failure process. In *Lockner et al.* [1991a, b], hypocentral locations were analyzed primarily to determine 1) the location and dimensions of the nucleation zone that marked the initiation of macroscopic failure and 2) the structure of the propagating fracture front that developed after nucleation. In the present paper, we will look in detail at the AE events leading up to fault nucleation in an attempt to observe precursory changes in the locations and amplitudes of these events.

EXPERIMENTAL PROCEDURE

Right cylinders of intact rock (Westerly granite and Berea sandstone) were precision ground to a length of 190.5 mm and a diameter of 76.2 mm. The sandstone had a porosity of 18%. Each sample was jacketed in a polyurethane tube and had six piezoelectric transducers (resonance at 0.6 MHz) attached to the rock surface to monitor stress-induced AE signals. Four additional transducers periodically measured the P-wave velocity field during each experiment to aid in the hypocentral inversion routine. Samples were deformed in a triaxial apparatus at constant confining pressure $P_c = 50.0 \pm 0.2$ MPa. Additional axial load was applied with a hydraulic ram controlled by a fast-acting valve and was automatically adjusted to maintain an approximately constant AE rate. This required reversing the ram during fault growth. Axial displacement was measured outside the pressure vessel while circumferential strain was measured with a foil strain gage attached to the mid-plane of the sample. This procedure and the hypocentral location scheme are described in more detail in *Lockner et al.* [1991a, b].

Location Accuracy

Since we will investigate patterns that develop in AE hypocentral locations prior to fault nucleation, it is important to know the location accuracy in our experiments. As we have discussed, the acquisition system is essentially the same as was used in past experiments in which the fracture nucleation process was studied [*Lockner and Byerlee*, 1980], as well as in a variety of other applications [e.g. *Lockner and Byerlee*, 1977; *Lockner et al.*, 1982]. To determine locations, AE signals are amplified and sent to a six channel monitoring system which stores the relative P-wave arrival times at the transducer sites as well as amplitude and first motion information. The arrival time data is later inverted to provide three dimensional locations for the source events. To aid in the event location analysis, the average P-wave velocity field [*Lockner et al.*, 1977] is determined independently during the course of the experiment by periodically measuring transit times of artificially generated acoustic pulses travelling along three different ray paths in the sample. Arrival time precision of the monitoring system sets a limit of ± 0.3 mm for the accuracy of determining source locations. However, in practice, other measurement errors further degrade the location accuracies. The primarily source of error is a tendency to systematically pick late arrivals for low-amplitude, emergent waveforms [*Lockner and Byerlee*, 1978]. The most convincing demonstration of the location accuracy has been the tight clustering of events on fault planes during fault propagation [*Lockner et al.*, 1991b], as shown in Fig. 3e. This empirical evidence suggests a location accuracy of less than 4 mm for larger amplitude events. A second way to demonstrate the performance of the automatic P-wave arrival detector is by plotting travel time residuals

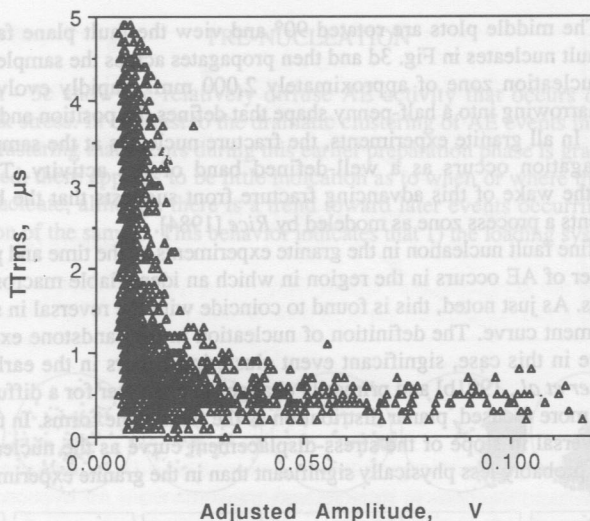


Figure 1. Performance of Location Algorithm. Travel time residuals TT_{rms} is less than 1 μs for events with amplitudes > 15 mV, resulting in location accuracies of ± 3 mm. Many smaller events give large residuals indicating that P-wave arrival was missed.

versus amplitude (Fig. 1). Large amplitude events are all located with rms travel time residuals $TT_{rms} < 1 \mu s$. However, below amplitudes of approximately 15 mV, TT_{rms} rapidly increases. This indicates that first arrivals of large events are successfully determined whereas small amplitude first arrivals are frequently missed, causing the location procedure to fail. A formal maximum likelihood estimate, using a 1 μs cutoff, actual transducer locations and representative events occurring in the central region of the sample, yields location errors of approximately ± 2 mm. This level of performance compares quite favorably with locations based on hand-picked arrivals [Lockner *et al.*, 1991b].

MACROSCOPIC FAULT GROWTH

A total of three granite and two sandstone samples have been tested. While those experiments are described in detail in Lockner *et al.* [1991b], we will focus mainly on results from one granite (G3) and one sandstone (S2) run. Stress-displacement curves for these two experiments are plotted in Fig. 2. In all granite experiments that have been performed, fault nucleation occurs abruptly at the reversal in slope of the stress-displacement curve. This macroscopic fault nucleation consistently occurs after, but near, peak stress. To illustrate this, a sequence of AE hypocentral locations for the granite experiment is plotted in Fig. 3. Events occurring in each time interval in Fig. 3 are shown in 3 projections. In the upper plots, the sample is viewed from the top. In the lower plots, the sample is viewed along-strike, so that the $\sim 68^\circ$ dip of the developing fault plane is

clearly seen. The middle plots are rotated 90° and view the fault plane face-on. The macroscopic fault nucleates in Fig. 3d and then propagates across the sample in Figs. 3e and 3f. The nucleation zone of approximately $2,000 \text{ mm}^3$, rapidly evolves into the nascent fault, narrowing into a half-penny shape that defines the position and orientation of the fracture. In all granite experiments, the fracture nucleates at the sample surface. Fracture propagation occurs as a well-defined band of AE activity. The relative quiescence in the wake of this advancing fracture front suggests that the band of AE activity represents a process zone as modeled by Rice [1984].

We will define fault nucleation in the granite experiments as the time and place where an abrupt cluster of AE occurs in the region in which an identifiable macroscopic fault zone first forms. As just noted, this is found to coincide with the reversal in slope of the stress-displacement curve. The definition of nucleation in the sandstone experiment is less clear, since in this case, significant event clustering occurs in the early stages of loading [Lockner *et al.*, 1991b] and primarily changes in character for a diffuse cloud of AE events to a more focused, planar distribution as the fault plane forms. In this case we will use the reversal in slope of the stress-displacement curve as the nucleation point, although this is probably less physically significant than in the granite experiments.

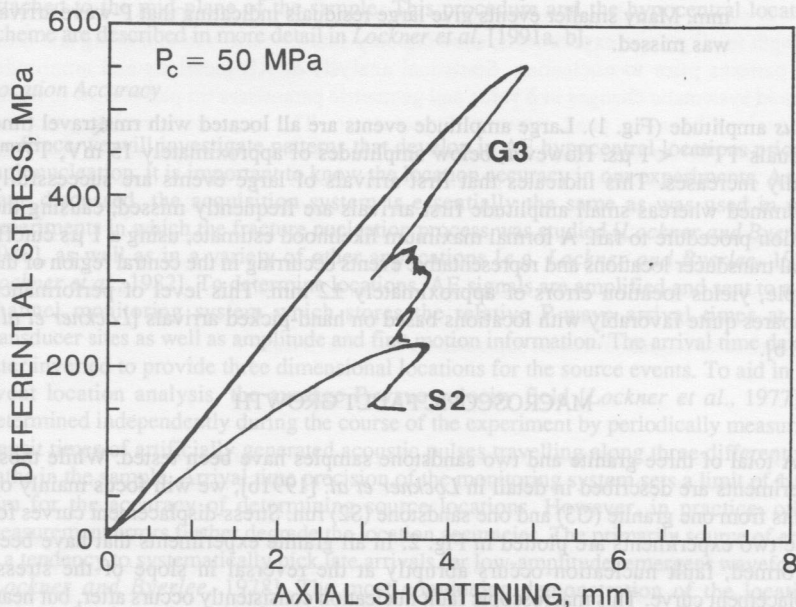


Figure 2. Stress-Displacement Plots. G3 is Westerly granite and S2 is Berea sandstone (18% porosity). Macroscopic fault nucleation occurs at reversal in slope after peak stress.

PRE-NUCLEATION

Figs. 3a - 3c show the relatively diffuse AE activity that occurs during loading through peak stress. In contrast to the dramatic clustering of AE events in the nucleation phase, the clustering that occurs during this earlier preparation phase is gradual and rather subtle. Indeed, there appears to be little indication as to when or where the macroscopic fault will nucleate, although there is a trend toward later events occurring more in the central region of the sample. This behavior indicates that 1) the loading system used in

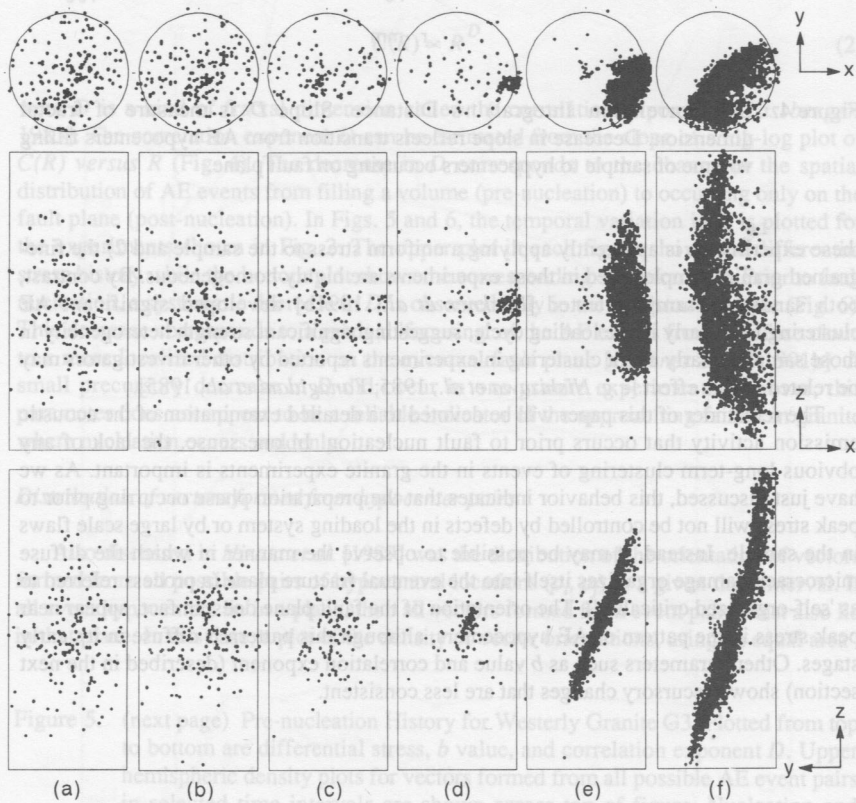


Figure 3. Macroscopic Fault Growth in Granite Sample G3. Sequential plots of AE hypocentral locations. a) early dilatancy; b) peak stress; c) 300 s interval before nucleation; d) 150 s interval after nucleation; e) 150 - 1150 s after nucleation; f) 4150 - 6150 s after nucleation. Bottom plots view sample along strike.

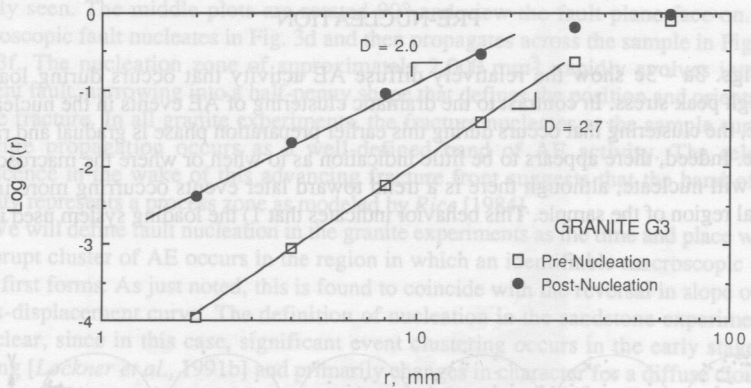


Figure 4. Log(Correlation Integral) vs Distance. Slope D is measure of fractal dimension. Decrease in slope reflects transition from AE hypocenters filling volume of sample to hypocenters occurring on fault plane.

these experiments is apparently applying a uniform stress to the sample and 2) the fine-grained granite samples used in these experiments are highly homogeneous. By contrast, both sandstone samples tested [Lockner *et al.*, 1991b] developed significant AE clustering from early in the loading cycle, suggesting significant strength heterogeneity in those samples. Early event clustering in experiments reported by other investigators may be related to this effect [e.g. Nishizawa *et al.*, 1985; Yanagidani *et al.*, 1985].

The remainder of this paper will be devoted to a detailed examination of the acoustic emission activity that occurs prior to fault nucleation. In one sense, the lack of any obvious long-term clustering of events in the granite experiments is important. As we have just discussed, this behavior indicates that the preparation phase occurring prior to peak stress will not be controlled by defects in the loading system or by large scale flaws in the sample. Instead, it may be possible to observe the manner in which the diffuse microcrack damage organizes itself into the eventual fracture plane (a process referred to as 'self-organized criticality'). The orientation of the fault plane does, in fact, appear near peak stress in the pattern of AE hypocenters, although this pattern is diffuse in its early stages. Other parameters such as b value and correlation exponent (described in the next section) show precursory changes that are less consistent.

Correlation integral

In searching for precursory variations in the AE data we will first consider variations in the spatial distribution of events. The first parameter that we will consider is the correlation integral $C(R)$ described by *Hirata et al.* [1987] as

$$C(R) = \frac{2}{N(N-1)} N_{(r < R)} \quad (1)$$

for a set of N hypocenters (p_1, p_2, \dots, p_N). In this case, $N_{(r < R)}$ is the number of pairs (p_i, p_j) separated by a distance smaller than R . If the distribution has a fractal structure, $C(R)$ is expressed by

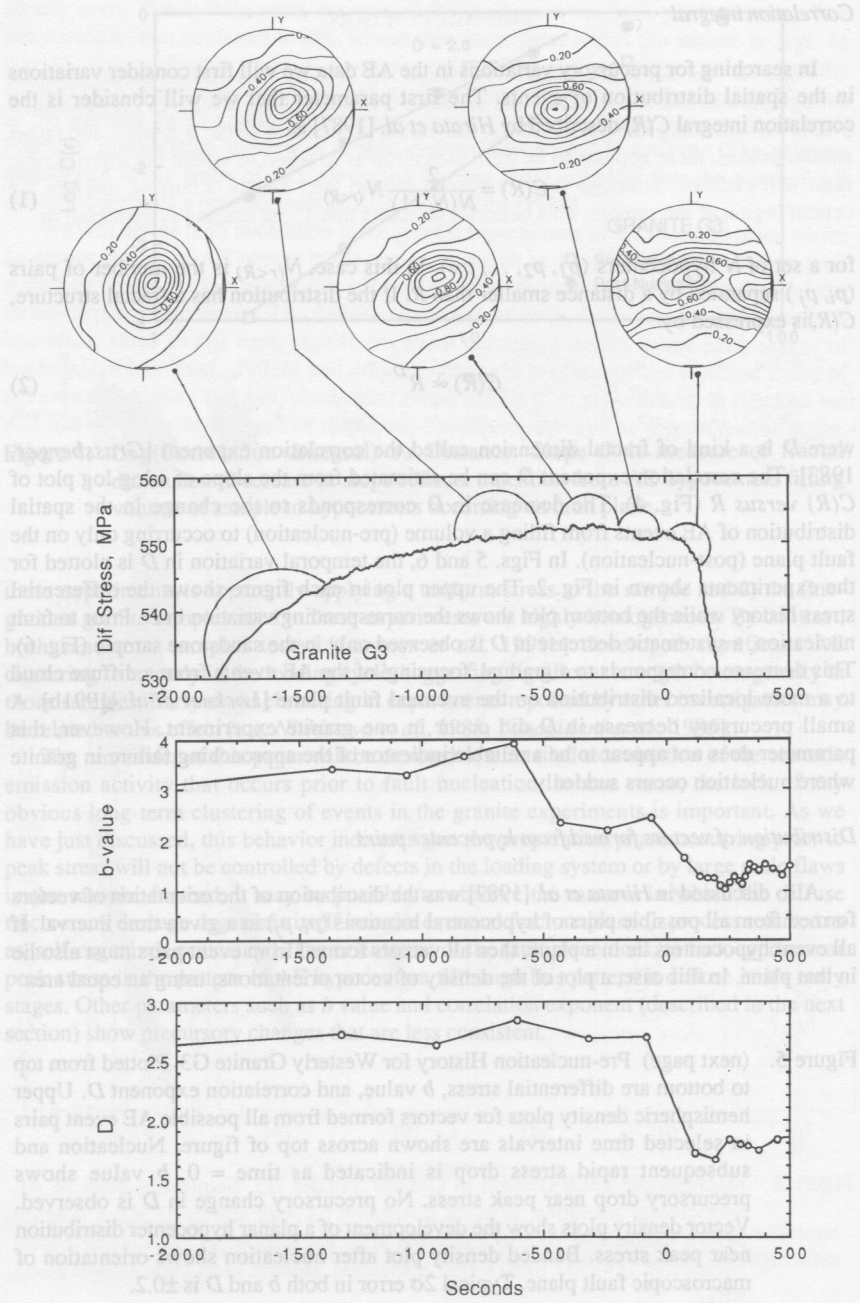
$$C(R) \propto R^D \quad (2)$$

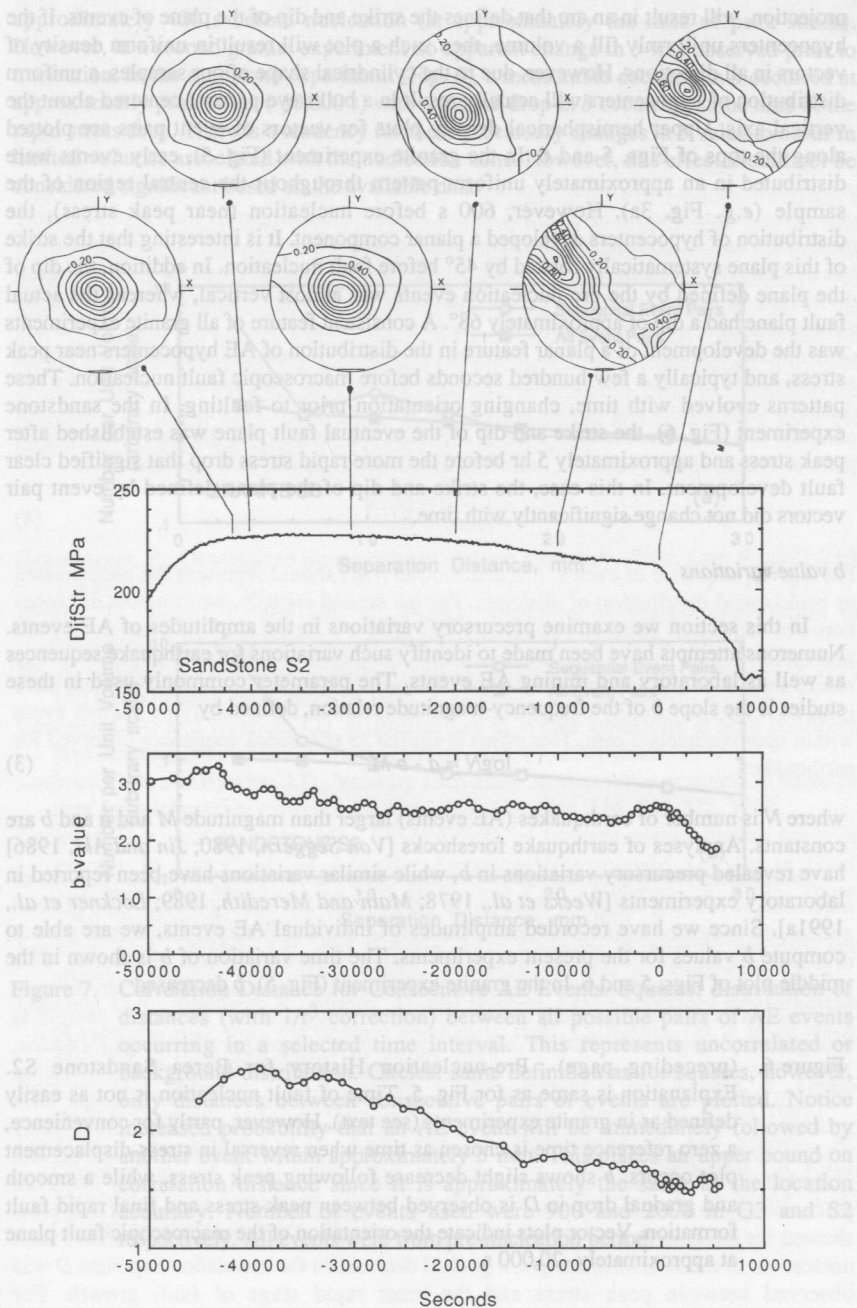
where D is a kind of fractal dimension called the correlation exponent [*Grassberger*, 1983]. The correlation exponent D can be estimated from the slope of a log-log plot of $C(R)$ versus R (Fig. 4). The decrease in D corresponds to the change in the spatial distribution of AE events from filling a volume (pre-nucleation) to occurring only on the fault plane (post-nucleation). In Figs. 5 and 6, the temporal variation in D is plotted for the experiments shown in Fig. 2. The upper plot in each figure shows the differential stress history while the bottom plot shows the corresponding variation in D . Prior to fault nucleation, a systematic decrease in D is observed only in the sandstone sample (Fig. 6). This decrease corresponds to a gradual 'focusing' of the AE events from a diffuse cloud to a more localized distribution on the eventual fault plane [*Lockner et al.*, 1991b]. A small precursory decrease in D did occur in one granite experiment. However, this parameter does not appear to be a reliable indicator of the approaching failure in granite where nucleation occurs suddenly.

Distribution of vectors formed from hypocenter pairs

Also discussed in *Hirata et al.* [1987] was the distribution of the orientation of vectors formed from all possible pairs of hypocentral locations (p_i, p_j) in a given time interval. If all event hypocenters lie in a plane, then all vectors formed from event pairs must also lie in that plane. In this case, a plot of the density of vector orientations, using an equal area

Figure 5. (next page) Pre-nucleation History for Westerly Granite G3. Plotted from top to bottom are differential stress, b value, and correlation exponent D . Upper hemispheric density plots for vectors formed from all possible AE event pairs in selected time intervals are shown across top of figure. Nucleation and subsequent rapid stress drop is indicated as time = 0. b value shows precursory drop near peak stress. No precursory change in D is observed. Vector density plots show the development of a planar hypocenter distribution near peak stress. Banded density plot after nucleation shows orientation of macroscopic fault plane. Typical 2σ error in both b and D is ± 0.2 .





projection, will result in an arc that defines the strike and dip of the plane of events. If the hypocenters uniformly fill a volume, then such a plot will result in uniform density of vectors in all directions. However, due to the cylindrical shape of our samples, a uniform distribution of hypocenters will actually result in a bull's eye pattern, centered about the vertical axis. Upper hemispherical density plots for vectors of event pairs are plotted along the tops of Figs. 5 and 6. In the granite experiment (Fig. 5), early events were distributed in an approximately uniform pattern throughout the central region of the sample (e.g. Fig. 3a). However, 600 s before nucleation (near peak stress), the distribution of hypocenters developed a planar component. It is interesting that the strike of this plane systematically rotated by 45° before fault nucleation. In addition, the dip of the plane defined by the pre-nucleation events was almost vertical, whereas the actual fault plane had a dip of approximately 68° . A consistent feature of all granite experiments was the development of a planar feature in the distribution of AE hypocenters near peak stress, and typically a few hundred seconds before macroscopic fault nucleation. These patterns evolved with time, changing orientation prior to faulting. In the sandstone experiment (Fig. 6), the strike and dip of the eventual fault plane was established after peak stress and approximately 5 hr before the more rapid stress drop that signified clear fault development. In this case, the strike and dip of the plane defined by event pair vectors did not change significantly with time.

b value variations

In this section we examine precursory variations in the amplitudes of AE events. Numerous attempts have been made to identify such variations for earthquake sequences as well as laboratory and mining AE events. The parameter commonly used in these studies is the slope *b* of the frequency-magnitude relation, defined by

$$\log N = a - b M \quad (3)$$

where *N* is number of earthquakes (AE events) larger than magnitude *M* and *a* and *b* are constants. Analyses of earthquake foreshocks [Von Seggern, 1980; Jin and Aki, 1986] have revealed precursory variations in *b*, while similar variations have been reported in laboratory experiments [Weeks et al., 1978; Main and Meredith, 1989; Lockner et al., 1991a]. Since we have recorded amplitudes of individual AE events, we are able to compute *b* values for the present experiments. The time variation of *b* is shown in the middle plot of Figs. 5 and 6. In the granite experiment (Fig. 5), *b* decreased

Figure 6. (preceding page) Pre-nucleation History for Berea Sandstone S2. Explanation is same as for Fig. 5. Time of fault nucleation is not as easily defined as in granite experiments (see text). However, partly for convenience, a zero reference time is chosen as time when reversal in stress-displacement plot occurs. *b* shows slight decrease following peak stress, while a smooth and gradual drop in *D* is observed between peak stress and final rapid fault formation. Vector plots indicate the orientation of the macroscopic fault plane at approximately -20,000 s.

approximately 400 s before nucleation (at approximately the time of peak stress). However, in a second granite experiment no apparent change in b was observed prior to nucleation. In the sandstone experiment (Fig. 6), a measurable decrease in b occurred at approximately peak stress (-40,000 s) with a second drop in b occurring at the time of the rapid stress drop. There is a tendency for these precursory changes in b value to occur in limited volumes associated with the nucleation zone. However, this effect should not be considered significant based on the available data.

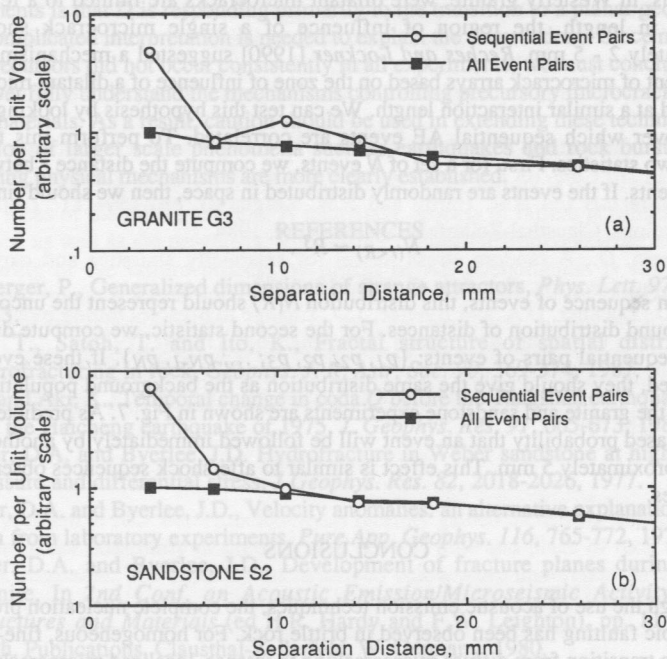


Figure 7. Correlation Distance for Consecutive AE Events. Squares: distribution of distances (with $1/r^3$ correction) between all possible pairs of AE events occurring in a selected time interval. This represents uncorrelated or background distribution. Circles: same definition as for squares, however, only distances between consecutive pairs of events are plotted. Notice increased probability that an AE event will be immediately followed by another event within approximately 5 mm. This places an upper bound on correlation distance since it is approximately the same as the location accuracy. Number of events used were 900 and 2000 in G3 and S2 respectively. All events were from pre-nucleation period.

Event correlation distance

While the correlation distance between successive AE events was not found to be a useful precursor to fault nucleation, it represents an important aspect of the spatial distribution of microcracking. The occurrence of an acoustic emission event represents the sudden release of strain energy; presumably due to microcrack growth. This must be accompanied by a redistribution of local stresses. Analysis of the stress field due to a crack [e.g. Segall and Pollard, 1980] shows that at distances greater than approximately three crack half lengths, perturbing stresses have dropped to less than 10% of the applied stress. Thus, in Westerly granite, where dilatant microcracks are limited to a few grain diameters in length, the region of influence of a single microcrack should be approximately 2 - 5 mm. Reches and Lockner [1990] suggested a mechanism for the development of microcrack arrays based on the zone of influence of a dilatant microcrack and arrived at a similar interaction length. We can test this hypothesis by looking for the distance over which sequential AE events are correlated. To perform this test, we compute two statistics. First, for a set of N events, we compute the distance r between all pairs of events. If the events are randomly distributed in space, then we should find

$$N(r < R) \propto R^3. \quad (4)$$

For a given sequence of events, this distribution $N(R)$ should represent the uncorrelated or background distribution of distances. For the second statistic, we compute distances between sequential pairs of events: $\{p_1, p_2; p_2, p_3; \dots; p_{N-1}, p_N\}$. If these events are uncorrelated, they should give the same distribution as the background population. The results for the granite and sandstone experiments are shown in Fig. 7. As predicted, there is an increased probability that an event will be followed immediately by another event within approximately 5 mm. This effect is similar to aftershock sequences observed for earthquakes.

CONCLUSIONS

Through the use of acoustic emission techniques, the complete nucleation process of macroscopic faulting has been observed in brittle rock. For homogeneous, fine-grained granite, the transition from diffuse microcracking to intense, localized microcrack growth in the nucleation zone occurred rapidly; in a matter of seconds to tens of seconds. This process may be better described in terms of cumulative crack damage. The relatively even distribution of AE hypocenters before nucleation suggests that the entire sample is brought very close to the critical damage state during the preparation stage [Madden, 1984]. Then the nucleation process rapidly increases the crack damage in the nucleation zone. In addition to this rapid onset of the macroscopic fault instability, longer term precursory variations in AE patterns could be identified. In general, these early precursors were first identifiable near the time of peak stress in granite experiments and preceded fault nucleation by a few hundred seconds. The most consistently observed precursor appeared in density plots of vectors generated from AE event pairs. These plots showed the development of planar distributions of AE event locations well before fault nucleation. In the sandstone sample, a gradual decrease in the correlation exponent D was observed between peak stress and the most rapid stage of fault growth. For

heterogeneous materials such as this sandstone, D should be a good indicator of the degree to which the early diffuse microcracking has organized into the early stage of fault formation. b value was also observed to decrease prior to fault nucleation in some experiments. However, this parameter would often show different trends for different sub-regions of the sample. We intend to examine this effect in more detail since spatial variations in b value may possibly be used to identify regions that are close to failure.

The vector plots, which showed the most consistent precursor, simply provide a convenient and sensitive method for detecting the transition from hypocenters filling a volume to their organizing into a planar structure. While in principle, D can provide information about the fractal distribution of events, our interpretation of the present experiments is that D is responding primarily to the transition to a planar geometry. No more complicated interpretation is needed to explain the observations. Since many of the early precursors did not occur consistently in all experiments, we must conclude that we do not yet fully understand the mechanisms controlling precursory microcrack growth in brittle materials. As a result, caution should be used in extending these techniques to the prediction of larger scale phenomena such as earthquakes and rock bursts until the underlying physical mechanisms are more clearly established.

REFERENCES

- Grassberger, P., Generalized dimensions of strange attractors, *Phys. Lett.* 97, 227-230, 1983.
- Hirata, T., Satoh, T. and Ito, K., Fractal structure of spatial distribution of microfracturing in rock, *Geophys. J. R. Astr. Soc.* 90, 369-374, 1987.
- Jin, A. and Aki, K., Temporal change in coda Q before the Tangshan earthquake of 1976 and the Haicheng earthquake of 1975, *J. Geophys. Res.* 91, 665-673, 1986.
- Lockner, D.A. and Byerlee, J.D. Hydrofracture in Weber sandstone at high confining pressure and differential stress, *J Geophys. Res.* 82, 2018-2026, 1977.
- Lockner, D.A. and Byerlee, J.D., Velocity anomalies: an alternative explanation based on data from laboratory experiments, *Pure App. Geophys.* 116, 765-772, 1978.
- Lockner, D.A. and Byerlee, J.D., Development of fracture planes during creep in granite, In *2nd Conf. on Acoustic Emission/Microseismic Activity in Geol. Structures and Materials* (ed H.R. Hardy and F.W. Leighton), pp. 11-25. Trans-Tech. Publications, Clausthal-Zellerfeld, W. Germany, 1980.
- Lockner, D.A., Walsh, J.B. and Byerlee, J.D., Changes in seismic velocity and attenuation during deformation of granite, *J. Geophys. Res.* 82, 5374-5378, 1977.
- Lockner, D.A., Summers, R., Moore, D. and Byerlee, J.D., Laboratory measurements of reservoir rock from the Geysers geothermal field, California, *Int. J. Rock Mech. Min. Sci. & Geomech. Abstr.* 19, 65-80, 1982.
- Lockner, D.A., Byerlee, J.D., Kuksenko, V., Ponomarev, A. and Sidorin, A., Quasi-static fault growth and shear fracture energy in granite, *Nature* 350, 39-42, 1991a.
- Lockner, D.A., Byerlee, J.D., Kuksenko, V., Ponomarev, A. and Sidorin, A., Observations of quasi-static fault growth from acoustic emissions, In *Fault Mechanics and Transport Properties of Rocks* (eds Evans, B. & Wong, T.-f.) (Academic Press) in press, 1991b.

- Madden, T.R., Microcrack connectivity in rocks: a renormalization group approach to the critical phenomena of conduction and failure in crystalline rocks, *J. Geophys. Res.*, 88, 585-592, 1984.
- Main, I.G. and Meredith, P.G., Classification of earthquake precursors from a fracture mechanics model, *Tectonophysics* 167, 273-283, 1989.
- Nishizawa, O., Onai, K. and Kusunose, K., Hypocenter distribution and focal mechanism of AE events during two stress stage creep in Yugawara andesite, *Pure Appl. Geophys.* 122, 36-52, 1985.
- Reches, Z. and Lockner, D.A., Self-organized cracking - a mechanism for brittle faulting, *EOS, Trans. American Geophys. Union* 71, 1586, 1990.
- Rice, J.R., Shear instability in relation to the constitutive description of fault slip, In *Proc. 1st Internat. Congress on Rockbursts and Seismicity in Mines, Johannesburg 1982*, pp. 57-62. SAIMM, Johannesburg, 1984.
- Segall, P. and Pollard, D., Mechanics of discontinuous faults, *J. Geophys. Res.* 85, 4337-4350, 1980.
- Terada, M., Yanagidani, T. and Ehara, S., A. E. rate controlled compression test of rocks, In *3rd Conf. on Acoustic Emission/Microseismic Activity in Geol. Structures and Materials* (ed H.R. Hardy and F.W. Leighton), pp. 159-171. Trans-Tech. Publications, Clausthal-Zellerfeld, W. Germany, 1984.
- Von Seggern, D., A random stress model for seismicity statistics and earthquake prediction, *Geophys. Res. Lett.* 7, 637-640, 1980.
- Weeks, J.D., Lockner, D.A. and Byerlee, J.D., Change in b-values during movement on cut surfaces in granite, *Bull. Seism. Soc. Amer.* 68, 333-341, 1978.
- Yanagidani, T., Ehara, S., Nishizawa, O., Kusunose, K. and Terada, M., Localization of dilatancy in Ohshima granite under constant uniaxial stress, *J. Geophys. Res.* 90, 6840-6858, 1985.